The Journal of Pathology: Clinical Research
J Pathol Clin Res November 2023; **9:** 464–474
Published online 9 August 2023 in Wiley Online Library (wileyonlinelibrary.com). DOI: 10.1002/cjp2.337

ORIGINAL ARTICLE

DNA methylation profile discriminates sporadic giant cell granulomas of the jaws and cherubism from their giant cell-rich histological mimics

Letícia Martins Guimarães[1], Daniel Baumhoer[2], Vanghelita Andrei[2], Dennis Friedel[3,4], Christian Koelsche[3,4,5,6], Ricardo Santiago Gomez[7], Andreas von Deimling[3,4*] and Carolina Cavalieri Gomes[1*]

[1]*Department of Pathology, Biological Science Institute, Universidade Federal de Minas Gerais (UFMG), Belo Horizonte, Minas Gerais, Brazil*
[2]*Bone Tumor Reference Centre, Institute of Pathology, University Hospital Basel and University of Basel, Basel, Switzerland*
[3]*Department of Neuropathology, Institute of Pathology, Heidelberg University Hospital, Heidelberg, Germany*
[4]*Clinical Cooperation Unit Neuropathology, German Cancer Research Center (DKFZ), German Consortium for Translational Cancer Research (DKTK), Heidelberg, Germany*
[5]*Department of General Pathology, Institute of Pathology, Heidelberg University Hospital, Heidelberg, Germany*
[6]*Institute of Pathology, Faculty of Medicine, LMU Munich, Munich, Germany*
[7]*Department of Oral Surgery and Pathology, School of Dentistry, Universidade Federal de Minas Gerais (UFMG), Belo Horizonte, Minas Gerais, Brazil*

**Correspondence to: Carolina Cavaliéri Gomes, Department of Pathology, Biological Sciences Institute, Universidade Federal de Minas Gerais (UFMG), Belo Horizonte, Minas Gerais, CEP 31270-901, Brazil. E-mail: gomes.carolinac@gmail.com, carolinacgomes@ufmg.br;*
Andreas von Deimling, Department of Neuropathology, Institute of Pathology, Ruprecht-Karls-University Heidelberg, D-69120 Heidelberg, Germany. E-mail: andreas.vondeimling@med.uni-heidelberg.de

Abstract

Sporadic giant cell granulomas (GCGs) of the jaws and cherubism-associated giant cell lesions share histopathological features and microscopic diagnosis alone can be challenging. Additionally, GCG can morphologically closely resemble other giant cell-rich lesions, including non-ossifying fibroma (NOF), aneurysmal bone cyst (ABC), giant cell tumour of bone (GCTB), and chondroblastoma. The epigenetic basis of these giant cell-rich tumours is unclear and DNA methylation profiling has been shown to be clinically useful for the diagnosis of other tumour types. Therefore, we aimed to assess the DNA methylation profile of central and peripheral sporadic GCG and cherubism to test whether DNA methylation patterns can help to distinguish them. Additionally, we compared the DNA methylation profile of these lesions with those of other giant cell-rich mimics to investigate if the microscopic similarities extend to the epigenetic level. DNA methylation analysis was performed for central ($n = 10$) and peripheral ($n = 10$) GCG, cherubism ($n = 6$), NOF ($n = 10$), ABC ($n = 16$), GCTB ($n = 9$), and chondroblastoma ($n = 10$) using the Infinium Human Methylation EPIC Chip. Central and peripheral sporadic GCG and cherubism share a related DNA methylation pattern, with those of peripheral GCG and cherubism appearing slightly distinct, while central GCG shows overlap with both of the former. NOF, ABC, GCTB, and chondroblastoma, on the other hand, have distinct methylation patterns. The global and enhancer-associated CpG DNA methylation values showed a similar distribution pattern among central and peripheral GCG and cherubism, with cherubism showing the lowest and peripheral GCG having the highest median values. By contrast, promoter regions showed a different methylation distribution pattern, with cherubism showing the highest median values. In conclusion, DNA methylation profiling is currently not capable of clearly distinguishing sporadic and cherubism-associated giant cell lesions. Conversely, it could discriminate sporadic GCG of the jaws from their giant cell-rich mimics (NOF, ABC, GCTB, and chondroblastoma).

Keywords: epigenetics; DNA methylation; copy number analysis; giant cell granulomas; cherubism; aneurysmal bone cyst; non-ossifying fibroma; giant cell tumour of bone; chondroblastoma; bone pathology

Received 5 March 2023; Revised 7 June 2023; Accepted 3 July 2023

No conflicts of interest were declared.

Introduction

Giant cell granulomas (GCGs) of the jaws often occur sporadically as localised central or peripheral lesions [1]. Less commonly, multifocal bone lesions microscopically indistinguishable from solitary GCG may develop in hyperparathyroidism or underlying syndromes, such as cherubism, Noonan syndrome, neurofibromatosis type 1, osteoglophonic dysplasia, cardiofaciocutaneous syndrome, oculoectodermal syndrome, and Jaffe–Campanacci syndrome [1,2]. Notably, in oculoectodermal and Jaffe–Campanacci syndromes, patients may develop multiple GCG of the jaws and non-ossifying fibromas (NOFs) of bone [3]. Sporadic GCG may have an indolent behaviour, but sometimes they can follow an aggressive clinical course and recur after conservative surgery [4]. Cherubism lesions tend to increase in the first years of life and regress after puberty. The disease shows variable expressivity, incomplete penetrance, and no clear genotype–phenotype correlation [5]. GCG and cherubism show similar microscopic features and are characterised by the proliferation of mononuclear cells and variable amounts of osteoclast-like giant cells in a haemorrhagic fibrovascular background [4,6,7].

Advances in next-generation sequencing technologies, as well as other gold-standard molecular techniques, have allowed a better understanding of the genetic basis of GCG [2]. We previously reported somatic, heterozygous, gain-of-function mutations in *KRAS*, *FGFR1*, and *TRPV4* in 72% of GCG [8]. Despite microscopic overlap, cherubism is characterised by mutations in the *SH3BP2* gene in 80–90% of cases [5,9].

Other tumours sharing histological features with GCG include NOF, aneurysmal bone cyst (ABC), giant cell tumour of bone (GCTB), and chondroblastoma [10,11]. Interestingly, microscopic similarities between GCG and NOF extend to a genetic level, since the same *KRAS* and *FGFR1* spectrum of mutations have been reported in extra-gnathic NOF in 78% of cases [11]. On the other hand, more than 90% of GCTB harbour *H3F3A* mutations, which are not found in GCG [12,13]. Additionally, chondroblastoma and ABC are characterised by *H3F3B* mutations and *USP6* rearrangements, respectively [12,14].

Although genetically characterised, the above-mentioned microscopically similar tumours have been poorly explored at the epigenetic level. DNA methylation is an epigenetic mechanism that plays an important role in normal mammalian development and disease, including cancer [15]. In translational terms, the study of the epigenetic basis of tumours is promising since DNA methylation is reversible and can be pharmacologically modified [16]. Over the past few years, DNA methylation profiling has been well established for the diagnosis of central nervous system tumours [17]. Additionally, machine learning approaches based on DNA methylation data have also been explored as potential tools for sarcoma classification [18,19].

Therefore, the present study aimed to assess DNA methylation profiles of central and peripheral sporadic GCG and cherubism to clarify if these lesions harbour similarities and cluster together or if they show completely distinct methylation profiles. We also compared the DNA methylation profiles of other giant cell-rich lesions, namely NOF, ABC, GCTB, and chondroblastoma, to assess whether they share similarities with GCG at the epigenetic level. In addition, we performed copy number analysis for all above-mentioned lesions.

Materials and methods

Patient sample selection

Ethics approval was granted by the Research Ethics Committee of Universidade Federal de Minas Gerais (protocol 44227021.4.0000.5149) and the study was conducted in accordance with the Declaration of Helsinki. Samples from giant cell lesions of the jaws were obtained from the oral pathology services from the authors' institution. The GCG had been previously assessed for genetic mutations [8]. Morphological re-examination and correlation with clinical data were conducted by oral pathologists to confirm the diagnosis. From the initial convenience sample of 30 archival formalin-fixed paraffin-embedded (FFPE) samples of giant cell lesions of the jaws (central = 10, peripheral = 10, and cherubism = 10), 4 samples could not be analysed due to limited genomic DNA (gDNA) availability or quality control (QC) failure, leaving 26 samples from 26 patients for analysis. Therefore, the final cohort consisted of 10 central GCG, 10 peripheral GCG, and 6 cherubism lesions (supplementary material, Table S1). In addition to the identification of mononuclear and osteoclast-like giant cells in a haemorrhagic fibrovascular background in H&E slides, the presence of multiple osteolytic lesions on radiographs, symmetric bone swelling since childhood, familial history of the disease, and normal parathormone levels were required for cherubism diagnosis [7].

Data from 45 samples of giant cell-rich histological mimics of giant cell lesions of the jaws were included for comparison: NOF ($n = 10$), ABC ($n = 16$), GCTB ($n = 9$), and chondroblastoma ($n = 10$) (supplementary material, Table S2). All the samples included in this study followed WHO criteria for diagnosis [3,20].

The methylation profiles of GCTB and chondroblastomas had been previously analysed [18]. To include samples processed in a single centre and under the same protocol, NOF of bone and ABC samples were evaluated for the first time in this study. With respect to these giant cell-rich lesions included for comparison with GCG and cherubism, ABC is rare, with estimated annual incidence of 0.15 per one million population [21], 1.5% of which occur in the jaws [20]. Based on this rarity, a single ABC case occurring in the mandible was included in the analysis. Approximately two-thirds of chondroblastoma involve the epiphyseal region of long bones, and occurrence in the craniofacial bones is exceptional [3]. Additionally, the authors did not have access to any case that could be unequivocally classified as NOF or GCTB occurring in the jaws. Notably, these tumours are not included in the WHO Classification of Head and Neck Tumours [20]. Therefore, the samples for comparison included NOF, GCTB, and chondroblastoma affecting the appendicular skeleton, both lower and upper limbs, and predominantly long bones. ABC samples included were from both the appendicular and axial skeleton. Although the brown tumour of hyperparathyroidism shares microscopic features with the above-mentioned tumours, it was not included in the analysis as it may easily be clinically distinguished by biochemical investigation.

DNA extraction, bisulphite conversion, and DNA methylation analysis

A representative region on an H&E section was identified and followed by taking a 1.5-mm punch from the corresponding site in the FFPE block for each sample. Only samples with a tumour content of at least 70% were included. gDNA was isolated from the FFPE samples using an automated Maxwell system and corresponding kits (Promega, Fitchburg, MA, USA). DNA quantification was performed with the Qubit dsDNA BR Assay Kit (Thermo Fisher Scientific, Waltham, MA, USA). Approximately 200 ng of gDNA from each sample was used for DNA bisulphite conversion, achieved with the EZ DNA Methylation-Gold™ Kit (Zymo Research, Irvine, CA, USA). DNA methylation analysis was performed using the Infinium Human Methylation EPIC (850K) Chip (Illumina, San Diego, CA, USA) to address 850,000 methylation sites across the genome, according to protocols supplied by the manufacturer. Subsequently, the chips were scanned with the iScan platform (Illumina).

The computational analyses were performed in R (http://www.R-project.org, R Development Core Team). Copy number alterations were investigated by applying the 'conumee' R package in Bioconductor (https://bioconductor.org/packages/release/bioc/html/conumee.html). Raw signal intensities were obtained from IDAT-files using the *minfi Bioconductor* package version 1.24.0. The procedure for data processing and downstream output after obtaining raw data from the methylation panels has been published elsewhere [17]. Summary copy number plots were generated using an in-house R-script (https://github.com/dstichel/CNsummaryplots).

Unsupervised analysis

Following QC, methylation data were analysed by unsupervised non-linear dimension reduction method Uniform Manifold Approximation and Projection (UMAP). The following parameters were used: number of CpGs = 20,000; nearest neighbours = 15; minimum distance between points = 0.25; spread of the clusters = 2; output dimensions = 2.

Unsupervised hierarchical clustering was carried out using the beta values of the 20,000 probes that show the highest median absolute deviation. Samples were hierarchically clustered using the Euclidean distance and Ward's linkage method. A heatmap shows the methylation levels varying from unmethylated state (blue colour) to methylated state (red colour).

Differential methylation of CpG sites and GO enrichment analysis

Estimation of differentially methylated positions (DMPs) analysis was done by using the functions from the R-package 'limma' [22]. The tests were carried out on the M values of the top 10,000 CpG positions ranked by variability. Relevant CpGs were defined when adjusted p value was smaller than 0.01 and a logfold-change larger than 2. Multiple testing correction was performed by using Benjamini Hochberg.

Box plots and Volcano plots were visualised using the R-package ggplot2 [23]. The Illumina Infinium HumanMethylationEPIC manifest was used to annotate CpGs of promoter and enhancer sites. CpGs in the Volcano plots are distributed according to their $-\log10$ adjusted p values and logfold-change. Top significant methylated CpGs are depicted in red, while the associated gene is shown for the top 100 DMPs. Evaluation and visualisation of overlapping differential methylated genes by Venn diagrams were done by using the R-package 'VennDiagramm' [24].

Gene ontology (GO) enrichment for significant CpGs from differential methylation analysis was carried out by using the gometh-function from the R-package 'missmethyl' [25].

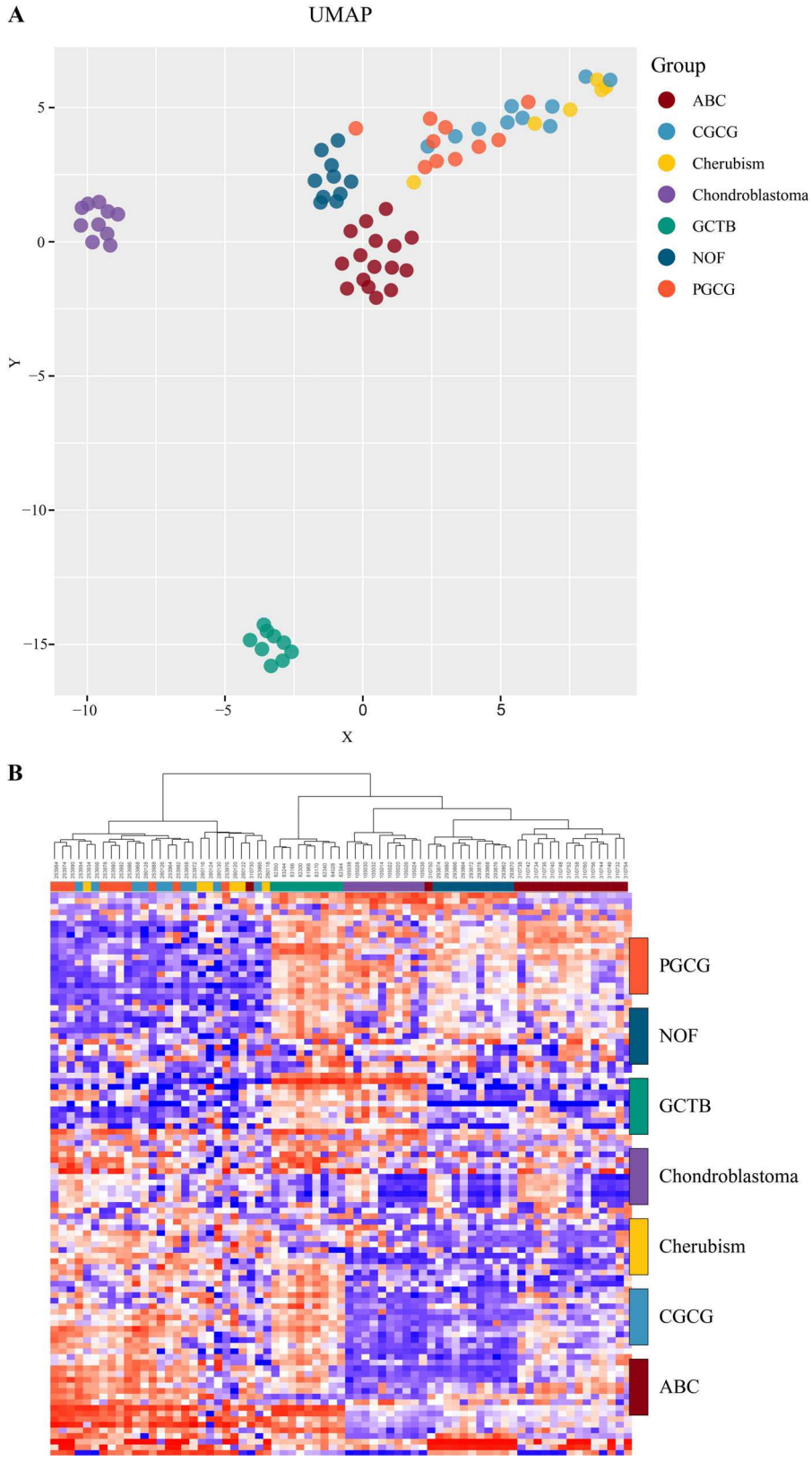

Figure 1. Legend on next page.

Results

Sample characterisation

The mean age of individuals with central GCG was 20.9 years (ranging from 7 to 53), while for the peripheral cases, it was 46.1 years (15–74) and for cherubism, 13.2 years. The male/female ratio was 2:3, 3:2, and 1:1, respectively. The mandible was the most commonly affected jawbone by peripheral GCG (8/10), cherubism (4/6), and central GCG (6/10). Available clinical information is shown in supplementary material, Table S1. The mutational status for sporadic GCG of the jaws previously assessed for genetic mutations [8] is listed in supplementary material, Table S1. Microscopically, all sporadic GCG and cherubism lesions had osteoclast-type multinucleated cells intermingled with ovoid or spindle-shaped mononuclear cells in a fibrovascular background with haemorrhage and hemosiderin deposition. Additionally, eosinophilic cuff-like perivascular deposits were identified in cherubism cases.

Available clinical information of giant cell-rich tumours included for comparison is shown in supplementary material, Table S2.

DNA methylation profiling

Sporadic central ($n = 10$) and peripheral ($n = 10$) GCG and cherubism ($n = 6$) cases generated DNA methylation profiling. To investigate whether sporadic GCG and cherubism share methylation common patterns with their histological mimics, methylation profiles of giant cell-rich lesions (NOF, ABC, GCTB, and chondroblastoma) were included, and DNA methylation data were analysed by UMAP and unsupervised hierarchical clustering.

Using the dimensionality reduction method, there was no unequivocal separation between sporadic GCG and cherubism by their DNA methylation profile (Figure 1). However, both UMAP analysis and unsupervised hierarchical clustering suggest different methylation patterns for peripheral GCG and cherubism, while central GCG intermingle with both (Figure 1). Notably, NOF, ABC, GCTB, and chondroblastoma revealed four distinct and individualised clusters (Figure 1). A similar clustering pattern as seen in the UMAP analysis is observed in t-distributed stochastic neighbour embedding (supplementary material, Figure S1).

Differential methylation of CpG sites and gene ontology enrichment analysis

Considering that central and peripheral sporadic GCG and cherubism share a related DNA methylation pattern, we evaluated the overall distribution of CpG methylation in functional regions and performed differential methylation analysis to assess DMP between these groups.

The global and enhancer-associated beta values showed a similar distribution pattern among the groups, with cherubism showing the lowest median CpG methylation values in these regions and peripheral GCG showing the highest. Conversely, the CpG DNA methylation values of promoter regions showed a different distribution pattern, with cherubism showing increased median methylation at promoters compared to both central and peripheral GCG (Figure 2A).

The differential methylation analysis revealed a significant number of differentially methylated genes only when comparing peripheral GCG versus cherubism ($n = 2{,}394$ genes) (Figure 2B). The most significantly differentially methylated genes between peripheral GCG and cherubism are highlighted in blue on the volcano plot (supplementary material, Figure S2). Although several GO terms were observed in the enrichment analysis, no term passed the false discovery rate (supplementary material, Table S3).

Copy number analysis

None of the samples included in the study (GCG, cherubism, NOF, ABC, GCTB, and chondroblastoma) exhibited a consistent pattern regarding gains or losses of chromosomal arms or segments (data not shown).

Figure 1. Unsupervised analysis of central giant cell granulomas of the jaws (CGCG), peripheral giant cell granulomas of the jaws (PGCG), cherubism, and their histological mimics, according to DNA methylation profile. (A) UMAP dimensionality reduction method and (B) unsupervised hierarchical clustering suggest that CGCG (light blue), PGCG (orange), and cherubism (yellow) share related DNA methylation patterns as they cluster together. However, PGCG of the jaws and cherubism seem slightly separated, indicating possible different methylation patterns, while CGCG intermingles with both groups. Further analyses with a larger cohort might help to resolve this. Interestingly, NOFs (dark blue) formed a distinct cluster from GCGs of the jaws, revealing that the genetic overlap does not extend to the methylation level. ABC (dark red), GCTB (green), and chondroblastoma (purple) form three individual clusters. The dendrogram depicts the results of unsupervised hierarchical clustering of methylation levels of the 20,000 probes that show the highest median absolute deviation across the beta values. The clinical group is indicated by colour. The level of DNA methylation (beta value) is represented with a colour scale varying from unmethylated state (blue colour) to methylated state (red colour).

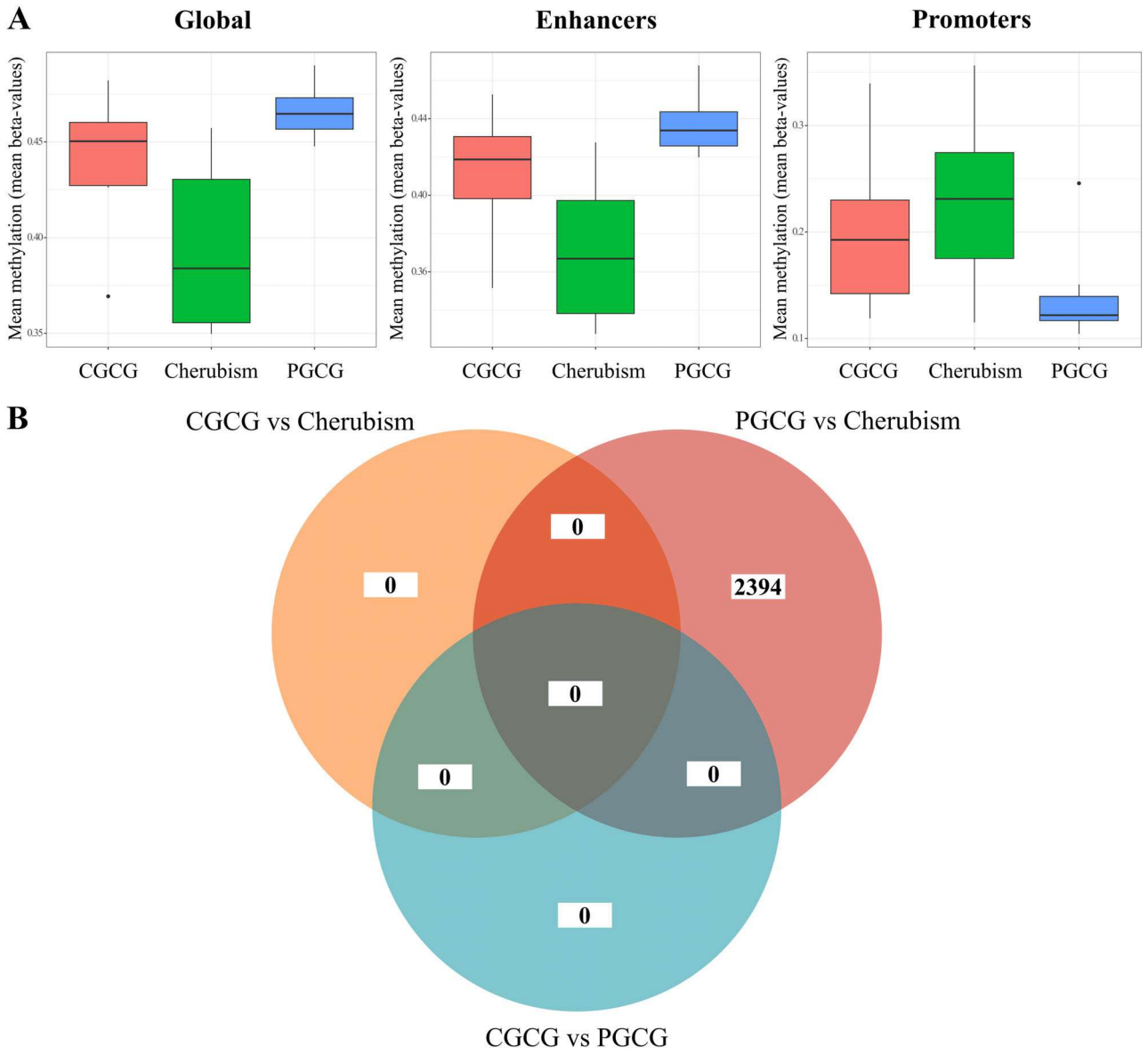

Figure 2. Comparison of methylation profiles between cherubism and sporadic GCGs of the jaws. (A) Boxplots depicting overall DNA methylation levels in giant cell-rich lesions of the jaws. Global, enhancer, and promoter-associated DNA methylation levels (beta values) of central giant cell granulomas of the jaws (CGCG), cherubism, and peripheral giant granulomas of the jaws (PGCG). (B) Venn diagram depicting the number of differentially methylated genes identified by differential methylation analysis across CGCG, PGCG, and cherubism. Statistically significant differentially methylated genes were observed between PGCG and cherubism.

Discussion

Recent development in epigenetic research has revealed that machine learning approaches based on DNA methylation are highly reliable in classifying central nervous system tumour diagnosis and to a lesser extent also bone and soft tissue tumours [17–19]. In addition to aiding diagnosis, epigenetic investigation has allowed the identification of novel tumour entities affecting the central nervous system [17,26]. DNA methylation analyses were also conducted to investigate if the epigenetic profile could be helpful to differentiate melanoma's site of origin in metastasis [27]. Notably, melanomas from different sites of origin (mucosal, conjunctival, and cutaneous melanomas) shared a common global DNA methylation profile, showing that global DNA methylation testing is not feasible to distinguish them. However, assessment at a gene level indicated that the frequencies of promotor

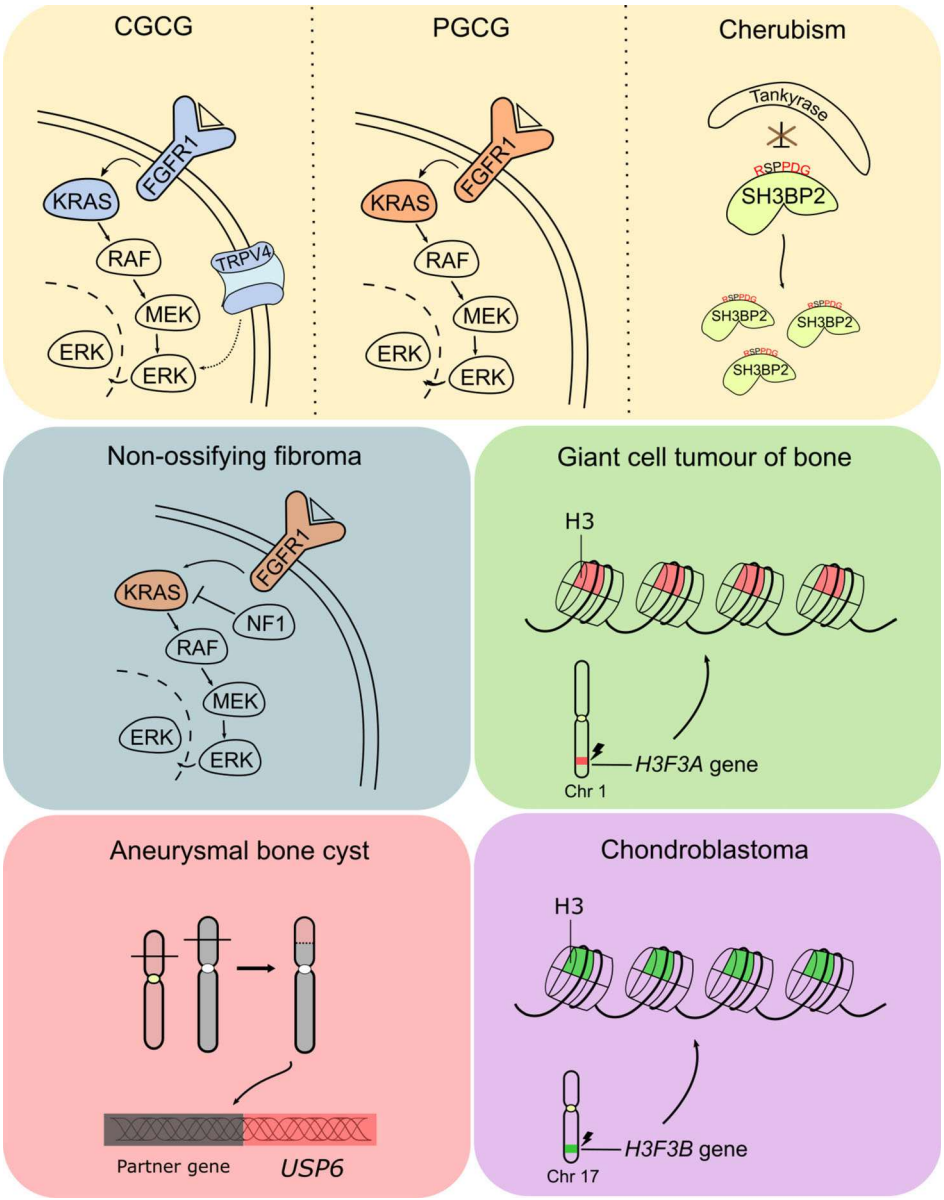

Figure 3. Genetic alterations of giant cell-rich tumours grouped based on their DNA methylation patterns. Central giant cell granulomas of the jaws (CGCG), peripheral giant granulomas of the jaws (PGCG), and cherubism are characterised by *KRAS/FGFR1/TRPV4*, *KRAS/FGFR1*, and *SH3BP2* mutations, respectively, and closely grouped in the methylation analysis (orange background). Although the role of SH3BP2 in establishing cherubism phenotype has not yet been elucidated, the loss of recognition site by Tankyrases proteins as a consequence of *SH3BP2* cherubism mutations was shown to be responsible for SH3BP2 accumulation in the cytoplasm and increased osteoclastogenesis [32,33]. Although PGCGs of the jaws and cherubism seem to cluster slightly separated, further analyses are needed to make it clearer. NOF of bone is closely related to sporadic GCGs of the jaws at a genetic level as it is characterised by *KRAS* and *FGFR1* mutations, in addition to *NF1* in cases associated with neurofibromatosis type I [11]. However, DNA methylation analysis separates NOF (blue background) from sporadic GCGs of the jaws. Finally, ABC, GCTB, and chondroblastomas, which are known by *USP6* rearrangements, *H3F3A* mutations, and *H3F3B* mutations, respectively, form three distinct and individualised clusters (red, green, and purple backgrounds).

methylation at specific cancer-related genes differ between primary melanoma sites [27]. Other than neoplasms, DNA methylation profiling has also been explored for classification in different contexts, such as malformations of the brain and reactive conditions (mesothelial reactive lesions) [28,29].

Herein, we explored and compared the DNA methylation patterns of osteoclast-like giant cell-rich lesions affecting the jaws, either sporadic or syndrome-associated, and their histological mimics. Our data show that sporadic central GCG shares a DNA methylation pattern with a fraction of their peripheral counterpart and with cherubism, whereas NOF, ABC, GCTB, and chondroblastoma have distinct patterns from GCG and cherubism.

DNA methylation plays a role in bone development and osteoclast differentiation [30,31]. *In vitro* experiments determined that DNA methylation (especially via *de novo* Dnmt3a) has an important role in RANKL-induced osteoclast differentiation from monocyte–macrophage lineage [31]. As DNA methylation is important in osteoclast differentiation and bone resorption under homeostatic conditions, it is plausible that epigenetic alterations are relevant to bone tumour pathogenesis, although such analysis is beyond the aim of this study. All tumours included in the present analysis are characterised by a variable amount of osteoclast-like multinucleate giant cells [10,11]. However, so far, the great majority of molecular investigations regarding these tumours have focused on genetic alterations (Figure 3).

Sporadic GCG is characterised by somatic, heterozygous, gain-of-function *KRAS*, *FGFR1*, and *TRPV4* mutations, which were detected in 72% (42/58) of cases [8]; specifically, *KRAS* p.G12D/A, p.G13D, p.A146V/P, p.V14L, p.L19F, and p.G10E mutations, *FGFR1* p.N330I and p.C381R, and *TRPV4* p.M713V/I mutations, with the latter exclusively detected in central lesions [8]. Such mutations are restricted to the mononuclear cells of the lesions [34], and converge to activation of MAPK/ERK signalling pathway [8]. No other pathogenic recurrent mutation could be identified in the remaining 30% of 'triple wild-type' cases [8]. Additionally, RNAseq revealed no fusions in GCG [8]. Notably, central and peripheral cases clustered together when DNA methylation profile was evaluated, irrespective of the genetic background (either *FGFR1*, *KRAS*, or *TRPV4* mutation-positive).

Despite microscopic similarities between the GCG of the jaws and cherubism, they are genetically distinct. *SH3BP2* exon 9 mutations are detected in 80–90% of cases of cherubism, affecting SH3BP2 protein residues 415, 418, 419, and 420 within a six-amino acid sequence (RSPPDG) (NM_001122681.2) [5,9]. Although SH3BP2 functions have not been entirely elucidated, plausible interactions of this protein with MAPK/ERK pathway have been raised by others [1], but such interactions remain untested. The *SH3BP2* gene contains C/G-rich regions and more than 42 CpG islands which are targets for gene regulation by DNA methylation, which likely makes it susceptible to regulation by epigenetic mechanisms [35]. Interestingly, the DNA methylation analysis shows that cherubism samples cluster together with central GCG, highlighting that the similarities extend from microscopic to the epigenetic level, despite genetic differences. It is of interest to follow up with larger cohorts to resolve the tendency of peripheral GCG to form a separate cluster, with central GCG and cherubism together forming another. Cherubism showed the lowest global and enhancer median CpG methylation values and the highest median CpG methylation values at promoter compared to both central and peripheral GCG. The biological significance of this methylation distribution remains to be further clarified.

Differentially methylated genes were only observed between peripheral GCG and cherubism, in line with what was observed in the unsupervised analysis. GO enrichment analysis was not able to identify signalling pathways differently affected by CpG methylation between these groups. Future studies, including larger cohorts, might be beneficial for differential methylation as well as GO enrichment analyses between these sporadic and syndromic lesions and may further refine their molecular pathogenesis.

NOF of bone shares histological and genetic similarities with sporadic GCG [2,11] but, herein, we demonstrate that they harbour distinct DNA methylation patterns. *KRAS* mutations (including the hot-spots p.G12A/D/V and p.G13D, and other variants p.K117N, p.A146P/T/V, p.Q61R/L, and p.A11Q) were reported in 64% of NOF of bone [11]. The same *FGFR1* mutations reported in sporadic GCG were detected in 14% of NOF [11]. Due to these overlapping genetic features, among other similarities, GCG and NOF of bone have previously been proposed to be part of the same spectrum disorder [2,36,37]. Remarkably, both UMAP analysis and unsupervised clustering were able to separate them. Notably, global DNA methylation analysis revealed that NOF and ABC presented distinct DNA methylation patterns, the latter being characterised by *USP6* rearrangements caused by chromosomal translocations involving 17p13 locus [14]. No fusion genes, including those involving *USP6* rearrangements, have been detected in sporadic GCG [8].

GCTB is characterised by *H3F3A* mutations, which have been reported in >90% of cases, with p.G34W being the most common mutation [12,38]. These mutations were confined to the 'stromal' mononuclear cell population rather than osteoclasts or their precursors [12]. Although H3.3 p.G34W mutation

affects a residue that does not undergo direct post-translational modification by histone methylation, it indirectly affects H3K36 and H3K27 methylation, leading to genome-wide epigenetic remodelling, crosstalk with DNA methylation, and GCTB tumourigenesis [39]. *H3F3A* mutations and other 15 H3 histone variant gene mutations have not been detected in sporadic GCG [8,13]. Unsupervised clustering of DNA methylation profiles revealed that GCTB is distinct from primary malignant p.G34 H3.3-mutated bone tumours [40]. Additionally, differential methylation analysis identified hypermethylation of *CCND1* promoter as specific for GCTB [40]. These results highlight the usefulness of DNA methylation analysis to predict aggressiveness in challenging diagnostic GCTB cases and its promising utility to identify epigenetic markers. In line with the discrepant clinical behaviour between GCTB and GCG, these tumours also have discrepant DNA methylation patterns.

GCTB and chondroblastomas form distinct DNA methylation clusters [40] (Figure 1). Similar to GCTB, chondroblastoma harbours histone H3.3 alterations [12,38]. However, *H3F3B* p.K36M is the most common mutation in chondroblastomas, detected in ∼90% of cases, while *H3F3A* p.K36M occurs in ∼10% of mutation-positive cases [12,38]. One may speculate that as there is crosstalk between DNA methylation and histone modification [41], and the specific mutations affecting glycine 34 or lysine 36 in histone H3.3 may be the reason for clear discrimination between GCTB and chondroblastoma by DNA methylation analysis. Additionally, the fact that mutations in genes encoding for histone H3.3 lead to genome-wide epigenetic alterations may also be the explanation for the dissociation of GCTB and chondroblastoma from the other bone tumours that do not harbour histone mutations.

One limiting factor in this study is that we compared GCG of the jaws and cherubism with other bone tumours occurring at different sites, including axial or appendicular skeleton. Such limitation, however, is inherent to the tumour types investigated. Many discoveries of new diagnostic markers derive from studies comparing the expression of RNA or proteins from samples from different locations. New studies adding samples of tumours occurring at the same location might further validate our results.

In conclusion, our results reveal that sporadic GCG of the jaws and cherubism-associated giant cell lesions share a related DNA methylation profile. Based on current morphological and molecular classification, DNA methylation testing does not contribute to separation of these entities, although peripheral GCG and cherubism appear to form different subgroups. Conversely, DNA methylation analysis could discriminate sporadic GCG from their giant cell-rich mimics, including NOF, ABC, GCTB, and chondroblastoma.

Acknowledgements

The authors thank the Coordination for the Improvement of Higher Education Personnel (CAPES)/Brazil, Fundação de Amparo à Pesquisa do Estado de Minas Gerais (FAPEMIG)/Brazil, and the National Council of Scientific and Technological Development (CNPq)/Brazil. LMG receives CAPES scholarship. RSG and CCG are research fellows at CNPq.

Author contributions statement

CCG and AvD conceived the study design. LMG, CCG, RSG, DB and VA selected samples. AvD supervised the experiments. LMG, CCG, AvD, DB, DF, CK and RSG performed data collection, data analysis and data interpretation. LMG and CCG wrote the first draft of the manuscript. AvD, DF and LMG generated figures. All authors were involved in writing the paper and had final approval of the submitted and published versions.

Data availability statement

The methylation data have been deposited in NCBIs Gene Expression Omnibus (http://www.ncbi.nlm.nih.gov/geo), with accession number GSE218252.

References

1. Schreuder WH, van der Wal JE, de Lange J, *et al*. Multiple versus solitary giant cell lesions of the jaw: similar or distinct entities? *Bone* 2021; **149**: 115935.
2. Gomes CC, Diniz MG, Bastos VC, *et al*. Making sense of giant cell lesions of the jaws (GCLJ): lessons learned from next-generation sequencing. *J Pathol* 2020; **25**: 126–133.
3. WHO Classification of Tumours Editorial Board. *Soft Tissue and Bone Tumours* (5th edn). International Agency for Research on Cancer: Lyon, 2020.
4. Jordan RC, Gomes CC, Gomez RS. Central giant cell granuloma. In: WHO Classification of Tumours Editorial Board (Ed). *Head and Neck Tumours* WHO Classification of Tumours Series, 5th edn; vol. **9**. Lyon: International Agency for Research on

Cancer; 2022 [Accessed 15 Aug 2022]. Available from: https://tumourclassification.iarc.who.int/chapters/52
5. Chrcanovic BR, Guimarães LM, Gomes CC, *et al*. Cherubism: a systematic literature review of clinical and molecular aspects. *Int J Oral Maxillofac Surg* 2021; **50**: 43–53.
6. Jordan RC, Gomes CC, Gomez RS. Peripheral giant cell granuloma. In: WHO Classification of Tumours Editorial Board (Ed). *Head and Neck Tumours*, WHO Classification of Tumours Series, 5th edn; vol. **9**. Lyon: International Agency for Research on Cancer; 2022 [Accessed 15 Aug 2022]. Available from: https://tumourclassification.iarc.who.int/chapters/52
7. Gomez RS, Flanagan AM. Cherubism. In: WHO Classification of Tumours Editorial Board (Ed). *Head and Neck Tumours*, WHO Classification of Tumours Series, 5th edn; vol. **9**. Lyon: International Agency for Research on Cancer; 2022 [Accessed 15 Aug 2022]. Available from: https://tumourclassification.iarc.who.int/chapters/52
8. Gomes CC, Gayden T, Bajic A, *et al*. TRPV4 and KRAS and FGFR1 gain-of-function mutations drive giant cell lesions of the jaw. *Nat Commun* 2018; **9**: 4572.
9. Ueki Y, Tiziani V, Santanna C, *et al*. Mutations in the gene encoding c-Abl-binding protein SH3BP2 cause cherubism. *Nat Genet* 2001; **28**: 125–126.
10. Flanagan AM, Speight PM. Giant cell lesions of the craniofacial bones. *Head Neck Pathol* 2014; **8**: 445–453.
11. Baumhoer D, Kovac M, Sperveslage J, *et al*. Activating mutations in the MAP-kinase pathway define non-ossifying fibroma of bone. *J Pathol* 2019; **248**: 116–122.
12. Behjati S, Tarpey PS, Presneau N, *et al*. Distinct H3F3A and H3F3B driver mutations define chondroblastoma and giant cell tumor of bone. *Nat Genet* 2013; **45**: 1479–1482.
13. Gomes CC, Diniz MG, Amaral FR, *et al*. The highly prevalent H3F3A mutation in giant cell tumours of bone is not shared by sporadic central giant cell lesion of the jaws. *Oral Surg Oral Med Oral Pathol Oral Radiol* 2014; **118**: 583–585.
14. Oliveira AM, His B-L, Weremowicz S, *et al*. USP6 (Tre2) fusion oncogenes in aneurysmal bone cyst. *Cancer Res* 2004; **64**: 1920–1923.
15. Greenberg MVC, Bourc'his D. The diverse roles of DNA methylation in mammalian development and disease. *Nat Rev Mol Cell Biol* 2019; **20**: 590–607.
16. Baylin SB, Jones PA. Epigenetic determinants of cancer. *Cold Spring Harb Perspect Biol* 2016; **8**: a019505.
17. Capper D, Jones DTW, Sill M, *et al*. DNA methylation-based classification of central nervous system tumours. *Nature* 2018; **555**: 469–474.
18. Koelsche C, Schrimpf D, Stichel D, *et al*. Sarcoma classification by DNA methylation profiling. *Nat Commun* 2021; **12**: 498.
19. Lyskjaer I, De Noon S, Tirabosco R, *et al*. DNA methylation-based profiling of bone and soft tissue tumours: a validation study of the 'DKFZ Sarcoma Classifier'. *J Pathol Clin Res* 2021; **7**: 350–360.
20. WHO Classification of Tumours Editorial Board. *Head and Neck Tumours* (5th edn). International Agency for Research on Cancer: Lyon, 2022.
21. Leithner A, Windhager R, Lang S, *et al*. Aneurysmal bone cyst. A population based epidemiologic study and literature review. *Clin Orthop Relat Res* 1999; **363**: 176–179.
22. Ritchie ME, Phipson B, Wu D, *et al*. limma powers differential expression analyses for RNA-sequencing and microarray studies. *Nucleic Acids Res* 2015; **43**: e47.
23. Wickham H. *ggplot2: Elegant Graphics for Data Analysis* (2nd edn). Springer: Cham, 2016.
24. Chen H. Package VennDiagram: Generate High-Resolution Venn and Euler Plots. 2022. [Accessed 20 May 2023]. Available from: https://cran.r-project.org/web/packages/VennDiagram/VennDiagram.pdf
25. Phipson B, Maksimovic J, Oshlack A. missMethyl: an R package for analyzing data from Illumina's HumanMethylation450 platform. *Bioinformatics* 2016; **32**: 286–288.
26. Perez E, Capper D. Invited Review: DNA methylation-based classification of paediatric brain tumours. *Neuropathol Appl Neurobiol* 2020; **46**: 28–47.
27. Jurmeister P, Wrede N, Hoffmann I, *et al*. Mucosal melanomas of different anatomic sites share a common global DNA methylation profile with cutaneous melanoma but show location-dependent patterns of genetic and epigenetic alterations. *J Pathol* 2022; **256**: 61–70.
28. Jabari S, Kobow K, Pieper T, *et al*. DNA methylation-based classification of malformations of cortical development in the human brain. *Acta Neuropathol* 2022; **143**: 93–104.
29. Bertero L, Righi L, Collemi G, *et al*. DNA methylation profiling discriminates between malignant pleural mesothelioma and neoplastic or reactive histologic mimics. *J Mol Diagn* 2021; **23**: 834–846.
30. de Andrés MC, Kingham E, Imagawa K, *et al*. Epigenetic regulation during fetal femur development: DNA methylation matters. *PLoS One* 2013; **8**: e54957.
31. Nishikawa K, Iwamoto Y, Kobayashi Y, *et al*. DNA methyltransferase 3a regulates osteoclast differentiation by coupling to an S-adenosylmethionine-producing metabolic pathway. *Nat Med* 2015; **21**: 281–287.
32. Guettler S, LaRose J, Petsalaki E, *et al*. Structural basis and sequence rules for substrate recognition by Tankyrase explain the basis for cherubism disease. *Cell* 2011; **147**: 1340–1354.
33. Levaot N, Voytyuk O, Dimitriou I, *et al*. Loss of Tankyrase-mediated destruction of 3BP2 is the underlying pathogenic mechanism of cherubism. *Cell* 2011; **147**: 1324–1339.
34. Miguita L, de Souza JC, Bastos VC, *et al*. Central giant cell granulomas of the jaws stromal cells harbour mutations and have osteogenic differentiation capacity, in vivo and in vitro. *J Oral Pathol Med* 2022; **51**: 206–216.
35. Fan C, Gaivin RJ, Marth TA, *et al*. Cloning and characterization of the human SH3BP2 promoter. *Biochem Biophys Res Commun* 2012; **425**: 25–32.
36. Bovée JV, Hogendoorn PC. Non-ossifying fibroma: a RAS-MAPK driven benign bone neoplasm. *J Pathol* 2019; **248**: 127–130.
37. Gomes CC, Gomez RS. MAPK pathway-activating mutations drive giant cell lesions of the jaws and non-ossifying fibromas of bone. *J Pathol* 2019; **248**: 123–124.

38. Presneau N, Baumhoer D, Behjati S, *et al*. Diagnostic value of H3F3A mutations in giant cell tumour of bone compared to osteoclast-rich mimics. *J Pathol Clin Res* 2015; **1**: 113–123.
39. Khazaei S, De Jay N, Deshmukh S, *et al*. H3.3 G34W promotes growth and impedes differentiation of osteoblast-like mesenchymal progenitors in giant cell tumor of bone. *Cancer Discov* 2020; **10**: 1968–1987.
40. Fittall MW, Lyskjaer I, Ellery P, *et al*. Drivers underpinning the malignant transformation of giant cell tumour of bone. *J Pathol* 2020; **252**: 433–440.
41. Moore LD, Le T, Fan G. DNA methylation and its basic function. *Neuropsychopharmacology* 2013; **38**: 23–38.

SUPPLEMENTARY MATERIAL ONLINE

Figure S1. t-Distributed stochastic neighbour embedding dimensionality reduction method showing a similar clustering pattern to UMAP based on DNA methylation profile

Figure S2. Volcano plots showing differentially methylated CpGs between central giant cell granulomas of the jaws (CGCG) versus cherubism, peripheral giant cell granulomas of the jaws (PGCG) versus cherubism, and CGCG versus PGCG

Table S1. Clinical and genetic data of sporadic central and peripheral giant cell granulomas of the jaws and cherubism

Table S2. Clinical data of giant cell-rich tumours that are histological mimics of giant cell granulomas of the jaws included for comparison

Table S3. GO enrichment analysis of peripheral giant cell granuloma versus cherubism